Identification of nonlinear bolted lap-joint parameters by force-state mapping

Hassan Jalali [a,1], Hamid Ahmadian [a], John E. Mottershead [b,*]

[a] *Department of Mechanical Engineering, Iran University of Science and Technology, Narmak, Teheran, Iran*
[b] *Department of Engineering, University of Liverpool, Brownlow Hill, Liverpool L69 3GH, UK*

Abstract

Joints and fasteners often have a significant effect on the dynamical behaviour of assembled mechanical structures and the analytical prediction of structural responses therefore depends upon the accuracy of joint modelling. Detailed constitutive models that fully describe the behaviour of frictional interfaces are often unduly complicated; in which case simpler phenomenological models having parameters identified from vibration tests may be preferable. Unfortunately the direct measurement of forces transmitted between two contacting surfaces and their relative displacements are not possible in practice and it is therefore necessary to rely on measurements remote from joints. In this paper, the parameters of an assumed nonlinear joint model are identified by force-state mapping from time-domain acceleration records in response to single-frequency excitation close to the first natural frequency. The problem of lack of accessibility for measurement at the joint is overcome by casting the governing equation of the system in modal coordinates so that modal parameters are identified to represent the nonlinear behaviour of the joint. A particular result from the experimental programme is the identification of viscous damping coefficients dependent upon displacement amplitude. The significance of this result is that the complex phenomenon of energy dissipation in lap joints can be represented by a simple analytical model capable of producing accurate results.
© 2007 Elsevier Ltd. All rights reserved.

Keywords: Bolted lap-joint; Force-state mapping; Damping; Hysteresis

1. Introduction

The behaviour of continuous materials in structural mechanics such as beams and plates is generally well understood. However, most practical structures are assemblies of many components and the connections between them are not well understood. This lack of understanding is important because the behaviour of the complete assembly, especially under dynamic loading conditions, can depend critically upon conditions

---

* Corresponding author. Tel.: +44 (0) 151 794 4827; fax: +44 (0) 151 794 4848.
  E-mail address: j.e.mottershead@liv.ac.uk (J.E. Mottershead).
[1] Visiting Researcher at the University of Liverpool.

existing at the connections. An important case in point is the preloading of bolted lap joints, which is known to affect the onset and extent of micro-slip and separation at interfaces. Slipping of contacting surfaces and the opening and closure of interfacial gaps are the predominant causes of nonlinearity and energy dissipation in built-up structures with bolted joints. Although much research has been carried out over many decades to understand joints and their effects, attention was drawn once again to this largely unsolved area of applied mechanics by the appearance of a US Department of Energy White Paper from Sandia National Laboratories (Dohner et al., 2000).

Many comprehensive review papers on joints and fasteners have appeared in recent years. Ferri (1995) considered the beneficial features of joint friction, namely damping and vibration isolation in a discussion focussed on the non-smooth representation of friction by the signum function and the hysteretic spring-friction model. Gaul and Nitsche (2001) and Segalman (2006) described a range of constitutive and phenomenological models, including finite-element whole-joint models and simpler representations based upon a analogy with material plasticity, typically Jenkins, Iwan, LuGre and Valanis models having a small number of parameters to be identified from vibration tests. Gaul and Nitsche (2001) described the semi-active damping of joints for vibration control applications. Berger's wide-ranging review of friction modelling (Berger, 2002) included a section on microslip, partial slip and passive damping, particularly relevant to joints. Ibrahim and Pettit (2005) drew attention to uncertainty in joints and concentrated their review upon bolted-joint stiffnesses and damping terms represented by random variables and fuzzy mathematics. They mentioned particularly the relaxation of preload with the passage of time and its uncertainty.

In the detailed finite element modelling of contacting frictional surfaces there are basically two approaches, based on finite-thickness and zero thickness interfaces. Typical modern examples include Ahmadian et al. (2006), who used thin-layer interface elements to model the large-area surface-to-surface joints between different components of the unclassified AWE MACE structure, and Mayer and Gaul (2007), who described segment-to-segment contact elements having the capability of both linear and nonlinear constitutive contact behaviour in normal and tangential directions, including nonlinear micro-slip behaviour. Mayer and Gaul's contact element included a Massing element (a variant of the Jenkins and Iwan models) to represent tangential contact behaviour.

The Iwan model is the most widely applied of the phenomenological interface models. Gaul and Lenz (1997) demonstrated that an adjusted version of it could represent the behaviour of lap joints. Their studies showed that hysteresis loops measured at different excitation force levels had different slopes; as the level of force increased, the slope of hysteresis loops decreased, indicating a softening nonlinearity. Ouyang et al. (2006) carried out an experimental study of the dynamic behaviour of a bolted structure under different levels of bolt preload and torsional excitation and demonstrated that experimental hysteresis loops were accurately reproduced when the joint was modelled using Jenkins elements. Song et al. (2004) proposed an adjusted Iwan element, taking the form of a beam, to simulate the nonlinear dynamic behaviour of bolted joints in beam structures. They extracted the joint parameters by using a multi-layer feed-forward neural network procedure. The capability of the model to represent nonlinear bolted-joint behaviour was confirmed by an experimental programme.

Other researchers have represented joints by nonlinear stiffness and damping terms (smooth or non-smooth) and applied classical perturbation methods. Various methods for the treatment of nonlinearity in structural dynamics are described in detail by Worden and Tomlinson (2001). In particular, Ferri and Bindemann (1992) considered vibrating systems with dry friction of different forms, such as friction dependent on displacement and velocity, friction where the normal force increases linearly with the slip displacement, and friction generated from active and passive structural joints. They used the first-order harmonic balance method to develop expressions for the equivalent natural frequencies and viscous damping ratios of beams with different types of frictional end conditions. Böswald and Link (2004) assumed a model for bolted joints consisting of a bilinear stiffness and a quadratic nonlinear damping function. The harmonic balance method was used to develop a mathematical model in the frequency domain having equivalent parameters identified using nonlinear frequency response functions from stepped sine tests. An application to the bolted flanges of aero-engine casings was considered. Ahmadian and Jalali (2007a) presented a parametric lumped model for the bolted lap joints consisting of a combination of linear and nonlinear springs with viscous damping. They used the method of multiple scales and derived a closed form solution for the nonlinear frequency response

function of an assembled beam structure containing a bolted lap joint at mid-span. They extracted the joint parameters by comparing the analytical and experimental frequency response curves. Later the same authors (Ahmadian and Jalali, 2007b) presented a generic element formulation consisting of a generic stiffness and a generic damping matrix to model the nonlinear behaviour of bolted lap joints. The resulting generic element was used in a FE model of a jointed beam structure and the analytical nonlinear frequency response functions were obtained by the incremental harmonic balance method. They then identified the joint parameters by minimising the difference between analytical nonlinear frequency response curves with their experimental counterparts.

Several recent experimental studies have been carried out providing important new results and understanding of bolted joints. Goege et al. (2005) presented a test strategy that can be used to identify and characterize nonlinear structural behaviour during modal testing. The method assumes a weakly nonlinear behaviour and operates in modal space. Ma et al. (2001) studied the effects of a lap joint placed between two cantilever beams while the assembly is excited using concentrated force acting parallel to the bolt axis. They treated the joint effect as an external force and identified the state of the joint from the difference between the dynamic response of the bolted structure and that of the corresponding monolithic structure (the same structure without the joint). Experiments were carried out on jointed and monolithic beams using non-contacting laser vibrometry. The identification revealed non-proportional damping and nonlinear softening effects due to micro-impact in the bolted joint. Smallwood et al. (2000) described a detailed experimental programme carried out on a carefully isolated shear joint. They showed that an equivalent viscous damping coefficient could be determined that increased with applied load; this result confirmed the findings of early research on structural joints by Ungar (1964, 1973). Another significant result was the energy dissipated at the joint was found to depend upon the applied external force according to a power law, $U = \alpha F^n$, where $2 < n < 3$. Hartwigsen et al. (2004) performed an experimental study to identify the principal joint effects on the structural dynamics of two structures composed of beam elements; a simple beam with the joint located at its centre and a rectangular frame with the joint in the centre of one of its longitudinal beams. A viscous damping ratio, being a function of vibration amplitude, was discovered to represent the frictional dissipation of energy at lap joints.

In this paper an assembled structure made up of two beams is connected by a bolted lap joint represented by a linear viscous damper and cubic stiffness. A finite element model of the beam and linear joint is updated using low-level vibration data. In the identification of the nonlinear joint, the assembled system, clamped at one end and free at the other, is excited at single frequencies in a band close to the first natural frequency under different bolt preload conditions and excitation levels. It is assumed that the displacement of the complete system is described by the first mode of vibration, and special care is taken in the experiment to ensure that this is so. The result is a single-degree of freedom nonlinear model in the first modal coordinate. Then, using the steady state response of the structure and employing force state mapping, the joint parameters (also in the first modal coordinate) are identified for different excitation frequencies. The need for direct force and displacement measurements at the joint is avoided by use of the updated linear model and modal coordinates. The results show that a cubic stiffness parameter may indeed be identified and that the linear damping coefficient depends upon the amplitude of displacement response. The latter result confirms the findings of the experimental study by Hartwigsen et al. (2004). A constraint is applied on energy dissipation as a power of the external load (Smallwood et al., 2000). Hysteresis loops generated from identified parameters are shown to agree well with hysteresis loops obtained directly from test measurements.

2. Joint modelling and identification

Fig. 1 shows an assembled structure consisting of two similar beams connected by a bolted lap joint. The equations governing the dynamic response of the system can be expressed in compact form as,

$$\mathbf{\Gamma d} = \mathbf{f}, \tag{1}$$

where $\mathbf{\Gamma}$ is an operator, $\mathbf{d}$ is the displacement field of the structure and $\mathbf{f}$ is the right hand side forcing vector, defined as,
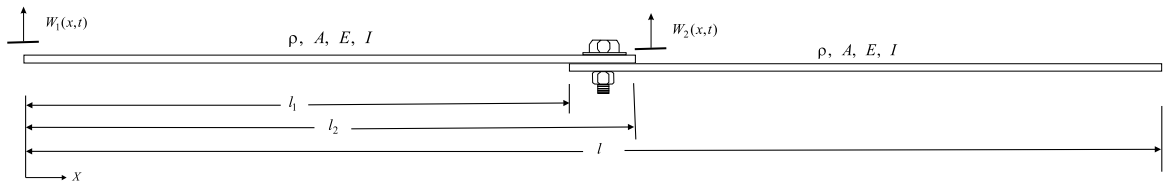
Fig. 1. The bolted beam structure.

$$\boldsymbol{\Gamma} = \begin{bmatrix} \boldsymbol{\Gamma}_{\mathrm{D}} \\ \boldsymbol{\Gamma}_{\mathrm{J}} \\ \boldsymbol{\Gamma}_{\mathrm{B}} \end{bmatrix}, \quad \mathbf{d} = \left\{ \begin{array}{c} W_1(x,t) \\ W_2(x,t) \end{array} \right\}, \quad \mathbf{f} = \left\{ \begin{array}{c} \bar{\mathbf{f}} \\ 0 \\ 0 \end{array} \right\}, \quad \bar{\mathbf{f}} = \left\{ \begin{array}{c} f_1(x,t) \\ f_2(x,t) \end{array} \right\}. \tag{2–5}$$

The operators $\boldsymbol{\Gamma}_{\mathrm{D}}$, $\boldsymbol{\Gamma}_{\mathrm{J}}$ and $\boldsymbol{\Gamma}_{\mathrm{B}}$ correspond, respectively, to the domain governing partial differential equations, compatibility requirements at the joint interface, and boundary conditions. These operators may be described separately as,

$$\boldsymbol{\Gamma}_{\mathrm{D}} = \begin{bmatrix} \rho A \frac{\partial^2}{\partial t^2} + EI\mathrm{D}^4 & 0 \\ 0 & \rho A \frac{\partial^2}{\partial t^2} + EI\mathrm{D}^4 \end{bmatrix}, \quad \boldsymbol{\Gamma}_{\mathrm{B}} = \begin{bmatrix} \delta(x)\mathrm{D}^2 & 0 \\ \delta(x)\mathrm{D}^3 & 0 \\ 0 & \delta(x-L)\mathrm{D}^2 \\ 0 & \delta(x-L)\mathrm{D}^3 \end{bmatrix}, \tag{6–7}$$

where $\mathrm{D}^n = \frac{\partial^n}{\partial x^n}$, and $\delta(x)$ is the Kronecker delta. The operator $\boldsymbol{\Gamma}_{\mathrm{B}}$ in Eq. (7) enforces the zero shear and bending moment at the boundaries. $\boldsymbol{\Gamma}_{\mathrm{J}}$, the joint operator, is a function of joint properties characterized by the joint mechanism. The operator that defines the joint between the two beams shown in Fig. 1 may be linear or non-linear or a combination of both. It describes the shear-force and bending-moment constitutional relationships. Joint modelling is concerned with identifying this operator qualitatively, which means making a decision about the form of the operator. Then, in joint identification it is attempted to clarify this operator quantitatively.

As an example, the linear spring-joint model shown in Fig. 2 may be described by an operator having the form,

$$\boldsymbol{\Gamma}_{\mathrm{J}} = \delta(L/2) \begin{bmatrix} EI\mathrm{D}^3 - k_{\mathrm{w}} & k_{\mathrm{w}} \\ k_{\mathrm{t}}\mathrm{D}^1 & EI\mathrm{D}^2 - k_{\mathrm{t}}\mathrm{D}^1 \end{bmatrix}. \tag{8}$$

The joint operator, $\boldsymbol{\Gamma}_{\mathrm{J}}$, enforces the requirements that the shear forces and bending moments in the beams at the joint interface are equal to the extension/compression force in the lateral spring, k_{w}, and the torque in the rotational spring, k_{t}.

Fig. 3 shows the generic joint element proposed by Ahmadian and Jalali (2007b). The operator governing the generic joint model is,
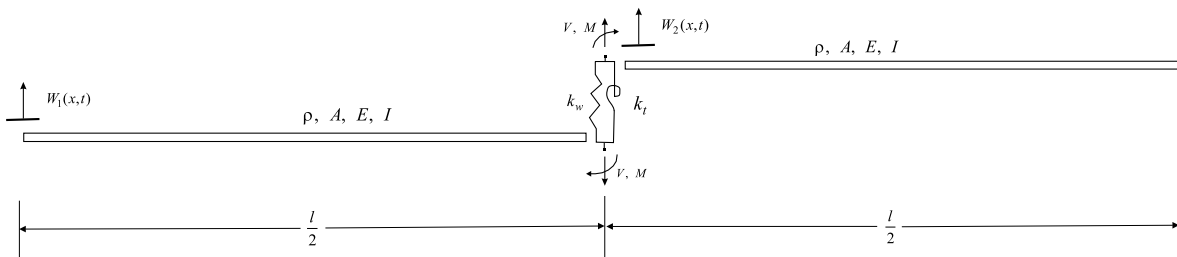

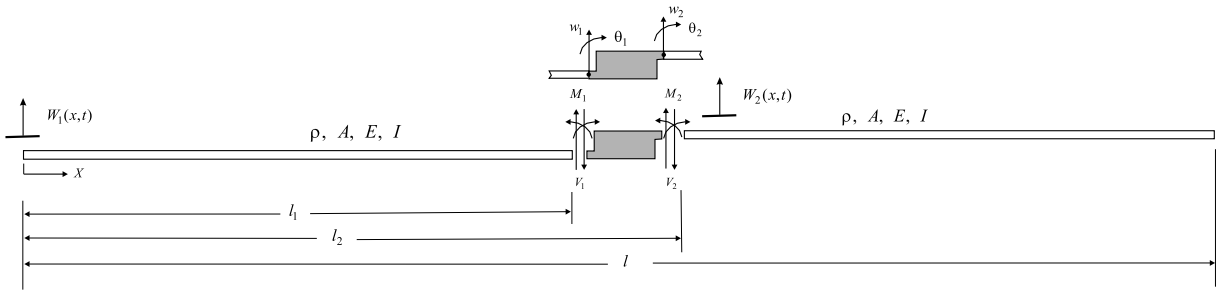Fig. 2. Lumped joint interface model.

Fig. 3. The generic joint element.

$$\Gamma_J = \left(\mathbf{M}_j\frac{d^2}{dt^2} + \mathbf{C}_j\frac{d}{dt} + \mathbf{K}_j\right)\begin{bmatrix} \delta(l_1) & 0 \\ \delta(l_1)\mathbf{D}^1 & 0 \\ 0 & \delta(l_2) \\ 0 & \delta(l_2)\mathbf{D}^1 \end{bmatrix} - EI\begin{bmatrix} \delta(l_1)\mathbf{D}^3 & 0 \\ \delta(l_1)\mathbf{D}^2 & 0 \\ 0 & \delta(l_2)\mathbf{D}^3 \\ 0 & \delta(l_2)\mathbf{D}^2 \end{bmatrix}. \tag{9}$$

The element has two nodes and terms relating to displacement, slope, shear force and bending moment are recognised immediately from Eq. (9). $\mathbf{M}_j, \mathbf{C}_j, \mathbf{K}_j$ represent the mass, damping and stiffness properties of the joint, so that in the case of a nonlinear joint $\mathbf{C}_j, \mathbf{K}_j$ may be regarded as displacement and velocity dependent functions. For example, Ahmadian and Jalali (2007a) considered a combination of cubic displacement and linear velocity functions to model the so-called 'slip' and 'slap' mechanisms. Song et al. (2004) used a model consisting of Jenkins elements and identified the joint parameters. Ma et al. (2001) treated the joint operator as an unknown external force at the joint location.

In cases where the beams and the joint are all modelled using finite elements the boundary conditions and the joint compatibility requirements are embedded in the model and operator Γ is then defined by,

$$\Gamma = \left(\mathbf{M}\frac{d^2}{dt^2} + \mathbf{C}\frac{d}{dt} + \mathbf{K}\right). \tag{10}$$

When the structure shown in Fig. 1 is excited by a single-frequency harmonic force close to the first natural frequency and the nonlinear joint model of Eq. (9) applies, then the response of the structure may be written in the form,

$$\mathbf{d}(x,t) = \varphi_1(x)q(t), \tag{11}$$

where $\varphi_1(x)$ is the first mode shape of the linear structure and $q(t)$ is a modal coordinate. Substituting Eq. (11) into Eq. (1), pre-multiplying by $\varphi_1(x)$ and integrating over the structure length, using the boundary conditions and mode-shape properties, leads after some algebraic manipulation (Appendix A) to,

$$\ddot{q}(t) + \omega_1^2 q(t) + [\varphi_J]\mathbf{f}_J = Q(t), \tag{12}$$

where $[\varphi_J] = [\varphi_1(l_1), \varphi_1'(l_1), \varphi_1(l_2), \varphi_1'(l_2)]$ contains the modal displacement and slopes at the joint interface and $\mathbf{f}_J$ is a vector containing the nonlinear parts of the shear forces and bending moments at the interface which are functions of the interface displacements and velocities,

$$\begin{Bmatrix} V_1 \\ M_1 \\ V_2 \\ M_2 \end{Bmatrix}_{nonlinear} = \begin{Bmatrix} f_1(d_J, \dot{d}_J) \\ g_1(d_J, \dot{d}_J) \\ f_2(d_J, \dot{d}_J) \\ g_2(d_J, \dot{d}_J) \end{Bmatrix}. \tag{13}$$

The first two expressions in Eq. (12) contain the information on the linear part of the assembled structure as well as the linear properties of the joint. The third expression contains the nonlinear joint information and is

generally a function of the joint element displacement and velocity. For the purposes of this analysis it is more convenient to cast Eq. (12) in the form,

$$\ddot{q}(t) + \omega_1^2 q(t) + h(\dot{q}, q) = Q(t), \tag{14}$$

which involves an assumption that the mode shape remains unchanged with vibration amplitude, i.e. the non-linearity affects the natural frequency but not the mode shape. The nonlinear function, $h(\dot{q}, q)$, in the modal domain, q, will be defined in the sequel using experimental observations by force-state mapping.

3. Force-state mapping

It is a common approach to identify the stiffness and damping properties of a nonlinear structure using force-state mapping (Masri and Caughey, 1979, 2004). Considering the equation of motion of the single degree of freedom nonlinear vibratory system given in Eq. (14), the restoring force may be obtained by subtracting the inertial force from the excitation force,

$$\omega_1^2 q(t) + h(q, \dot{q}) = Q(t) - \ddot{q}(t). \tag{15}$$

The time histories of the displacement and its derivatives and of the applied forces are assumed to be known. From Eq. (15), it is possible to find the restoring force defined as $Q(t) - \ddot{q}(t)$. Having the restoring force and using the displacement and velocity signals the system parameters may be identified.

Al-Hadid and Wright (1990) used ordinary polynomials as well as special terms to describe non-smooth nonlinearities. Such mathematical forms were not only able to describe meaningful physical behaviour, therefore termed parametric, but also were shown to provide a better fit to experimental restoring forces than the previously used orthogonal polynomials, termed nonparametric. The same authors (Al-Hadid and Wright, 1992) applied their method to an experimental T-beam structure with bending and torsional modes having damping and stiffness nonlinearity.

In practice, it is common to measure the applied force and acceleration and estimate the velocity and displacement by integration. The resulting displacement and velocity signals may suffer from phase distortion due to the integration procedure. Also there is a possibility of phase distortion between measured force and acceleration signals, but with modern measurement equipment this later type of phase distortion is usually reduced to very small levels. The damping coefficient is very sensitive to phase distortion in integrated signals, small levels of which may result in a 100% change in an identified damping coefficient (Meskell and Fitzpatrick, 2001, 2002). Therefore special care should be taken in estimating the velocity and displacement signals. Worden (1990a) considered the problem of data processing in the restoring force surface method. This paper is concerned with determining which signal – displacement, velocity or acceleration—should be measured and which numerical integration and/or differentiation procedure should be used to determine the two others. Worden showed that numerical integration procedures can be used to reliably produce estimated velocity and displacement data from acceleration measurement by a variety of methods but the numerical differentiation is less reliable. In a companion paper (Worden, 1990b) the same author examined the reliability of using numerical integration by using noisy experimental data. The results indicate that integration procedures appear to be insensitive to measurement noise.

In this paper, the steady state response of the structure is used in force-state mapping and the system parameters are identified. In order to eliminate any phase distortion in numerically integrated displacement and velocity signals a single-frequency harmonic excitation is used. The response of the structure will be harmonic too and generally contains higher harmonics in the response due to the nonlinearity. Considering that the excitation frequency is ω, the measured acceleration signal may be represented using,

$$\ddot{q}(t) = \sum_{i=1}^{n} (A_n \sin(n\omega t) + B_n \cos(n\omega t)). \tag{16}$$

Writing Eq. (16) in each time instant and using a least-square procedure the coefficients A_n and B_n may be identified. Once the coefficients of Eq. (16) are known, the velocity and displacement are obtained by analytical integration,

$$\dot{q}(t) = \sum_{i=1}^{n} \frac{1}{n\omega}(-A_n \cos(n\omega t) + B_n \sin(n\omega t)) + C_1 \tag{17}$$

$$q(t) = \sum_{i=1}^{n} -\frac{1}{(n\omega)^2}(A_n \sin(n\omega t) + B_n \cos(n\omega t)) + C_1 t + C_2. \tag{18}$$

The mean values of the velocity and displacement signals have to be zero, which means that $C_1 = 0, C_2 = 0$.

4. Numerical example

A single degree of freedom nonlinear system governed by the following equation was considered,

$$\ddot{q}(t) + c_{eq}\dot{q}(t) + \omega_1^2 q(t) - k_3 q^3(t) = Q(t)$$
$$\omega_1 = 170.0, \quad k_3 = 5 \times 10^6, \quad Q(t) = \sin(\omega t). \tag{19}$$

Following Hartwigsen et al. (2004), the equivalent viscous damping, c_{eq}, was considered to be dependent upon the maximum amplitude of the steady state response, q_{max}. We assume,

$$c_{eq} = c_0 + c_1 q_{max} + c_2 q_{max}^2$$
$$c_0 = 0.08, \quad c_1 = 70.0, \quad c_2 = 1 \times 10^4. \tag{20}$$

The excitation frequency was varied in a frequency band around the natural frequency of the linear system and time-domain responses were determined using a Runge–Kutta procedure. An iterative approach was used to solve Eq. (19). An initial value was considered for q_{max} and the steady state amplitude was obtained. Using the steady state amplitude a new value for q_{max} was calculated. After several iterations q_{max} converged to a constant value. The nonlinear frequency response function of the system was obtained by using the amplitude of the steady-state simulated response at each excitation frequency as in Fig. 4.

At each excitation frequency the steady state acceleration and the corresponding applied force (in the same time interval) were used and the restoring force was calculated using $Q(t) - \ddot{q}(t)$. By employing Eq. (16) the governing equation of the steady state acceleration was estimated and the coefficients A_n and B_n were calculated. With these coefficients known and by using Eqs. (17) and (18) the velocity and displacement of the steady state response were calculated. Having displacement, velocity and restoring force signals it was possible to calculate the system parameters. Two different models were considered for the system, expressed in the following equations,
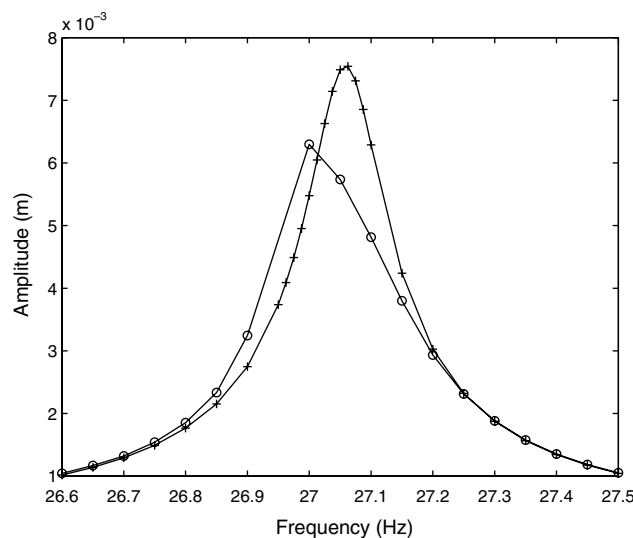

Fig. 4. Frequency response curves, (+) linear system, (○) nonlinear system.

$$Q(t) - \ddot{q}(t) = \omega_1^2 q(t) - k_3 q^3(t) + c_{eq}\dot{q}(t) \tag{21}$$

$$Q(t) - \ddot{q}(t) = \omega_1^2 q(t) - k_3 q^3(t) + c_{eq}\dot{q}(t) + c_1|\dot{q}(t)|\dot{q}(t) + c_2\dot{q}(t)^3. \tag{22}$$

Given Eq. (21) as system model, the unknown parameters were identified by using the following equation,

$$\begin{Bmatrix} \omega_1^2 \\ k_3 \\ c_{eq} \end{Bmatrix} = \begin{bmatrix} q(t_1) & -q^3(t_1) & \dot{q}(t_1) \\ q(t_2) & -q^3(t_2) & \dot{q}(t_2) \\ \vdots & \vdots & \vdots \\ q(t_n) & -q^3(t_n) & \dot{q}(t_n) \end{bmatrix}^{\dagger} \begin{Bmatrix} Q(t_1) - \ddot{q}(t_1) \\ Q(t_2) - \ddot{q}(t_2) \\ \vdots \\ Q(t_n) - \ddot{q}(t_n) \end{Bmatrix}, \tag{23}$$

where $(\bullet)^{\dagger}$ denotes the pseudo inverse. In Table 1 the identified and exact parameters are compared. The identified parameters in Table 1 were the averages of the identified parameters over the excitation frequency band shown in Fig. 4, where the linear and nonlinear frequency response curves are seen to deviate from each other.

Fig. 5 shows the identified parameters for different excitation frequencies. The identified values for ω_1 and k_3 are seen to be almost constant over the excitation frequency band but the equivalent damping coefficient, c_{eq}, is not constant, as expected.

The discrete points shown in Fig. 6 are the values of c_{eq} determined at the separate test frequencies with different vibration amplitudes, q_{max}. The fitted curve is plotted using the identified damping coefficients, c_0, c_1 and c_2, given in Table 2. The figure clearly shows that the equivalent damping coefficient is dependent upon the maximum response amplitude, q_{max}, as was intended from Eq. (20).

Table 1
Exact and identified parameters for: $\omega_1^2 q(t) - k_3 q^3(t) + c_{eq}\dot{q}(t)$

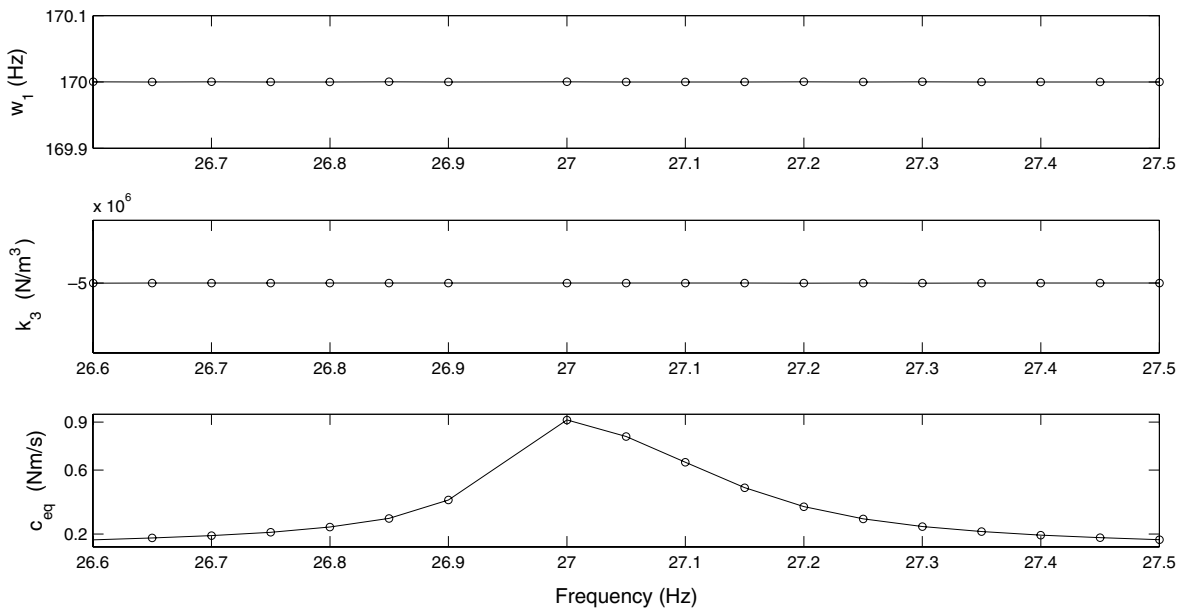|	ω_1 (Hz)	k_3 (N/m^3)
Exact	170.0	5×10^6
Identified	170.0	5×10^6
Error (%)	0.0	0.0

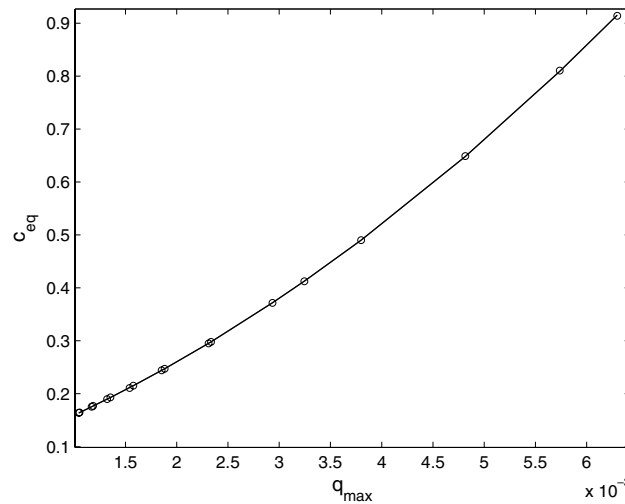Fig. 5. Identified parameters for $\omega_1^2 q(t) - k_3 q^3(t) + c_{eq}\dot{q}(t)$.

Fig. 6. Equivalent damping coefficient c_{eq}, identified (points) and fitted (full line).

Table 2
Exact and identified damping parameters for: $c_{eq} = c_0 + c_1 q_{max} + c_2 q_{max}^2$

	c_0	c_1	c_2
Exact	0.080	70.0	1×10^4
Identified	0.078	71.12	9.795×10^3
Error (%)	2.5	1.6	2.05

Table 3
Exact and identified parameters for: $\omega_1^2 q(t) - k_3 q^3(t) + c_{eq}\dot{q}(t) + c_1|\dot{q}(t)|\dot{q}(t) + c_2\dot{q}(t)^3$

	ω (Hz)	k_3 (N/m^3)	c_1	c_2
Exact	170.0	5×10^6	0.0	0.0
Identified	170.0	5×10^6	-7.7×10^{-9}	1.3×10^{-8}
Error (%)	0.0	0.0	–	–

The same procedure was applied for the model defined by Eq. (22). Table 3 compares the exact and identified parameters. Again the parameters shown in Table 3 are the average of identified parameters over the excitation frequency band.

Results presented in Tables 1–3 show that the force state mapping method has the capability to identify system parameters with high precision. In the following sections an experimental case study of two beams connected by a bolted lap-joint is considered.

5. Experiment

The experimental bolted joint coupling two identical steel beams is pictured in Fig. 7. The structural parameters of the beams were given by $L = 0.42$ cm (overall length), $b = 2.54$ cm (width) and $h = 0.636$ cm (thickness). The fixed-free boundary condition was chosen and the structure was excited by a concentrated external force applied by an electromagnetic shaker through a stinger at position $x = 5$ cm, as shown in Fig. 8. The excitation point was chosen to be close to the fixed end in order to minimise any unwanted nonlinearities arising in the magnetic field of the shaker should the armature undergo large displacements when the beam was in resonance, thereby causing a distorted force signal. It was important to keep the excitation signal clear of the higher harmonics as much as possible. Bucher (1998) proposed an iterative algorithm that
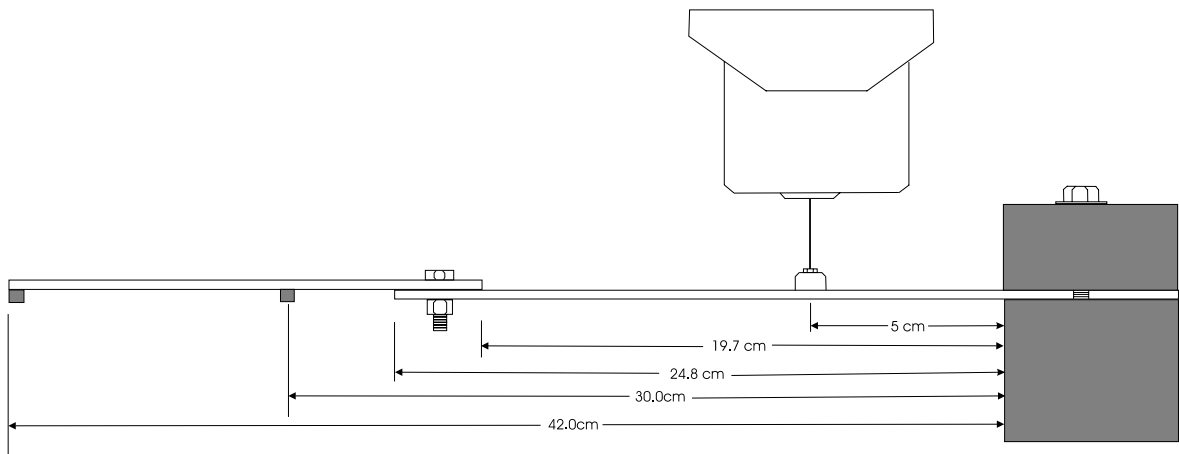
Fig. 7. Test set-up.

Fig. 8. Structure geometrical arrangement.

can be used to excite a nonlinear structure with a pure sine excitation signal. The force applied to the structure was measured with force transducer. Two accelerometers were used in positions $x = 30$ cm and $x = 42$ cm to measure the response. A force cell placed under the bolt head made it possible to measure the bolt preload and to carry out the experiment for different known preloads. The measured data were analysed using an LMS CADA-X system.

The experiments were completed for two bolt preloads, 120 and 540 N. At each preload three different excitation levels were used, $F = 1.5$ N, $F = 3$ N and $F = 6$ N. First the structure was excited by using a low-level random excitation signal and linear frequency response functions (FRFs) were measured. The linear FRFs corresponding to the accelerometer placed at $x = 42$ cm are pictured in Fig. 9. Table 4 shows the three first experimental natural frequencies. The linear natural frequencies were used to update a linear finite element model of the beams and linear spring connection by adjusting the joint stiffness coefficients. It was assumed that finite element model of the beam sections of the structure were correct and that the beam formed an ideal cantilever with fixed-free end conditions. The finite element model consisted of 35 identical Euler–Bernoulli beam elements having two degrees of freedom per node and one generic element (Ahmadian and Jalali, 2007b). The experimental mode shapes and the mode shapes obtained from identified FE model were in excellent agreement. It is a crucial point that the updated finite element mass-normalised mode shape is accurate since the modal coordinate q was determined from $\mathbf{d} = \{\varphi_1\}q$ using just two accelerometers.
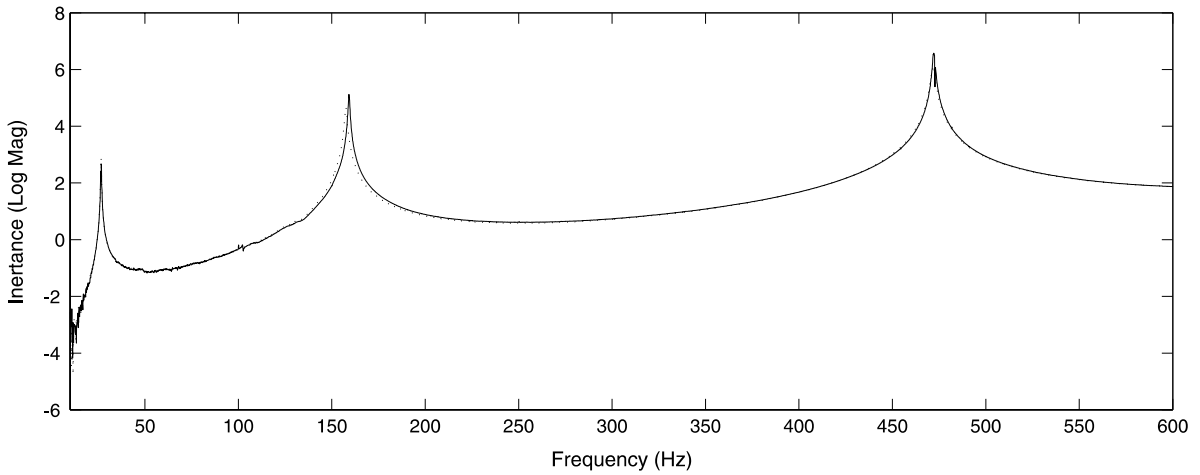
Fig. 9. Linear frequency response functions at different preloads: 120 N (dashed line) and 540 N (solid line).

Table 4
Linear natural frequencies

	ω_1 (Hz)	ω_2 (Hz)	ω_3 (Hz)
120 N	26.4	157.6	471.8
540 N	26.6	159.1	472.4

In the second stage of experiment, the structure was excited using a harmonic force, the excitation frequency being chosen to vary in a frequency band close to the first natural frequency. The excitation amplitude was maintained at a constant level for all excitation frequencies, the steady state response of the structure and its corresponding force signal were recorded and the nonlinear FRFs obtained. These are shown in Fig. 10 and correspond to the accelerometer closest to the tip of the beam. The nonlinear structural parameters were identified from the time-domain signals. The measured preload was found to remain unchanged after each experiment, which seems reasonable since the preload was high, the frequency was low and the applied sinusoidal forces were low.
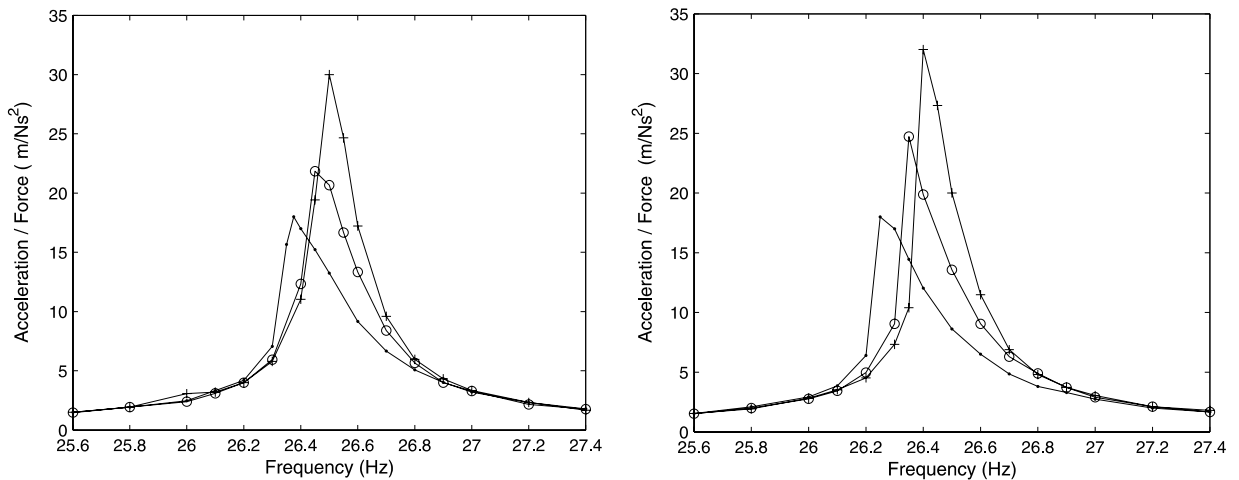

Fig. 10. Nonlinear FRFs at different preloads (120 N (left) and 540 N (right)) and excitation levels: $F = 1.5$ N (+), $F = 3$ N (o) and $F = 6$ N (•).

6. Parameter identification

In order to identify the system parameters a decision must firstly be made on the form of the function governing the joint dynamics $h(q,\dot{q})$. In this case the function was defined based on experimental observation. Fig. 10 indicates a softening effect in the response and therefore a cubic displacement function was used to represent the joint stiffness. A linear viscous damper was included to allow for energy dissipation. The nonlinear function describing the joint physics was therefore described by,

$$h(q,\dot{q}) = c\dot{q} - k_3 q^3. \tag{24}$$

The unknown parameters of Eq. (23) were identified using the experimental results obtained in the previous section for each excitation frequency. In previous sections it was assumed that the structure responds in its first mode, but in reality higher modes of the structure participate in the response too. The higher modes were eliminated by application of Eq. (12) enabling the dynamics to be represented by Eq. (13) in the first modal coordinate. The first mode shape was determined from the updated finite element model using the linear system (low excitation level) frequency response function data. Higher harmonics were truncated in the filtered acceleration signal by using Eq. (16) and selecting $n = 4$. The restoring force vector was calculated using the modal acceleration and force signals $\ddot{q}(t)$ and $Q(t)$ and employing $Q(t) - \ddot{q}(t)$. The displacement and velocity signals, needed to determine the constitutive joint parameters by Eq. (23), were determined by analytical integration as described in Section 3. Fig. 11 shows a typical measured force, acceleration and the corresponding calculated
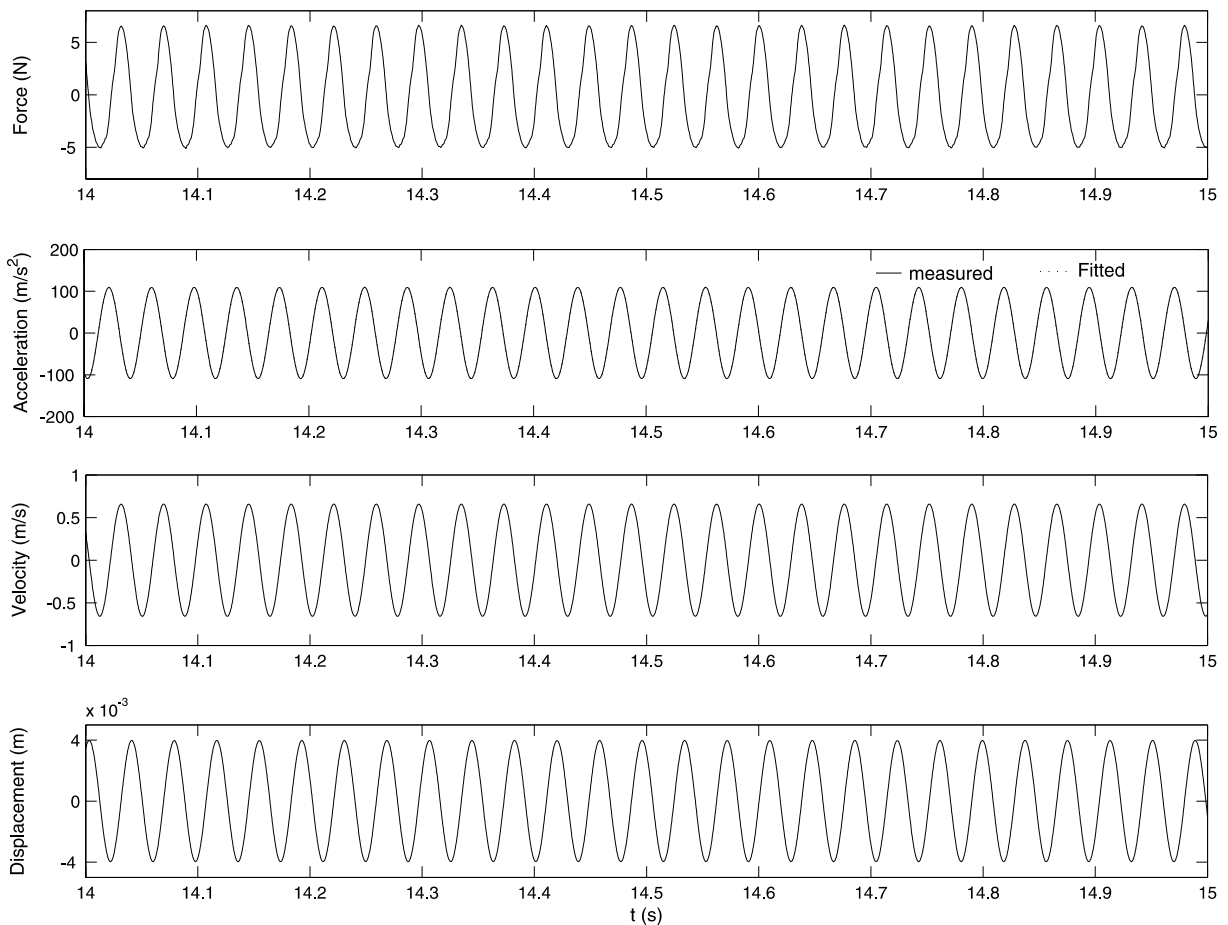

Fig. 11. Applied force, acceleration and analytically determined velocity and displacement signals at preload 540 N and $F = 6$ N.

velocity and displacement signals. As this figure shows, the measured and fitted acceleration signals were in good agreement.

Given Eq. (24) as the joint model and by using Eq. (23) the unknown parameters were identified for each excitation frequency. Table 5 compares the identified nonlinear stiffness coefficient, k_3, and natural frequencies, ω_1, for different preloads and different excitation amplitudes. The natural frequencies and nonlinear stiffness coefficients shown in Table 5 are the average values over the excitation frequency band.

Table 5 shows that at each bolt preload the identified natural frequency remains almost constant and as the bolt preload increases the natural frequency increases too, the result of an increase in system stiffness. At the highest excitation level ($F = 6$ N) the natural frequency is unchanged showing, as one might expect, that the preload effect is less significant at higher excitation levels. The identified nonlinear stiffness coefficient is also almost constant for the lower bolt preload, and at the higher preload remains closely constant at the two lower excitation levels. When compared to the higher k_3 values (at low preload) the lower values (at high preload) do not seem to be too dissimilar bearing in mind the difficulties in identifying them. As the bolt preload increases the nonlinearity decreases.

The identified damping coefficients are shown in Fig. 12. Unlike the natural frequency and nonlinear stiffness coefficient, which were expected to be constant for each preload, the identified damping coefficient is not constant for different excitation frequencies at each preload. Fig. 12 shows that as the response amplitude increases, the damping coefficient increases too. This indicates that the damping in the lap joints is dependent upon the maximum displacement amplitude and should be modeled as $c = f(q_{max})$.

In this paper Eq. (21) is now re-written in the form,

$$Q(t) - \ddot{q}(t) = \omega_1^2 q(t) - k_3 q(t)^3 + c(q_{max})\dot{q}(t), \qquad (25)$$

where $c(q_{max}) > 0$ is a positive definite function and $q_{max} > 0$ is the deformation amplitude at each load level for each excitation frequency. The adopted damping is a function of the maximum displacement in the joint and may be defined as:

$$c(q_{max}) = c_0 + c_1 q_{max} + c_2 q_{max}^2 + \cdots \qquad (26)$$

Table 5
Identified nonlinear stiffness coefficient and natural frequency

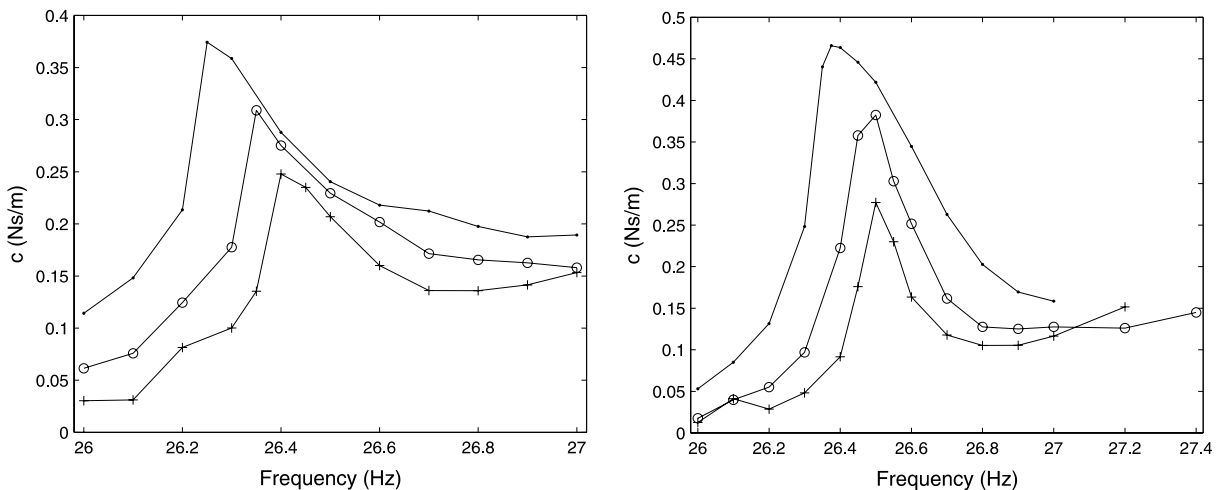| Preload (N)	ω (Hz)			k_3 (N/m^3)		
	$F = 1.5$ N	$F = 3$ N	$F = 6$ N	$F = 1.5$ N	$F = 3$ N	$F = 6$ N
120	26.48	26.49	26.47	6.721×10^7	7.087×10^7	5.450×10^7
540	26.55	26.59	26.46	2.168×10^7	2.180×10^7	1.167×10^7

Fig. 12. Identified damping coefficients: 120 N (left) and 540 N (right): $F = 1.5$ N (+), $F = 3$ N (o) and $F = 6$ N (•).

As the bolt preload changes the damping properties of the joint and the energy dissipated in the joint interface changes. The selected polynomial makes it possible to choose different damping functions for different bolt preloads. For a fully tightened bolt with linear behaviour the damping function is linear i.e. $c(q_{max}) = c_0$, which gives a good representation of the actual damping behaviour. As the bolt preload decreases the nonlinearity of the damping function governing the joint interface increases. Therefore a higher order polynomial must be used for the damping function. There is a constraint on choosing the order of the polynomial given by the energy dissipated at the joint interface. Experimental investigations (Smallwood et al., 2000; Ungar, 1964) show that the energy dissipation, U, vs. the amplitude of the applied external force, F, follows a power-law relationship as $U = \alpha F^n$, where $2 < n < 3$. The selected damping function should be able to regenerate the energy dissipation in the joint interfaces according to the given power law. For the experimental results shown in Fig. 12, first and second order polynomials are chosen as damping functions for two different bolt preloads, e.g. 540 and 120 N, respectively.

Experimental investigations by Hartwigsen et al. (2004) showed that for a chosen bolt preload damping in bolted lap joints is dependent upon displacement amplitude. Curves representing the damping function $c(q_{max})$ are shown in Figs. 13 and 14.

For each of the identified models (6 models obtained from 2 different preloads and three excitation force levels) the dissipation energy vs. input force is calculated and shown in Figs. 15 and 16. Having identified the damping coefficients in Figs. 13 and 14 and by using the steady-state response, the damping force is calculated for one cycle using $F_d(t) = c(q_{max})\dot{q}(t)$. The energy dissipated over one period of vibration is then determined according to $\int_0^T F_d(t)\dot{q}(t)dt$, which is solved numerically. The index n is between 2.36 and 2.39 for the joint with preload of 120 N and it is increased to 2.52–2.59 for preload of 540 N.

The experimental and analytical hysteresis loops are shown in Figs. 17 and 18 at chosen excitation frequencies. The linear stiffness contribution to modal restoring force is omitted to that the remaining figure allows for a very clear comparison of the nonlinear stiffness and damping effects. The experimental hysteresis loops,
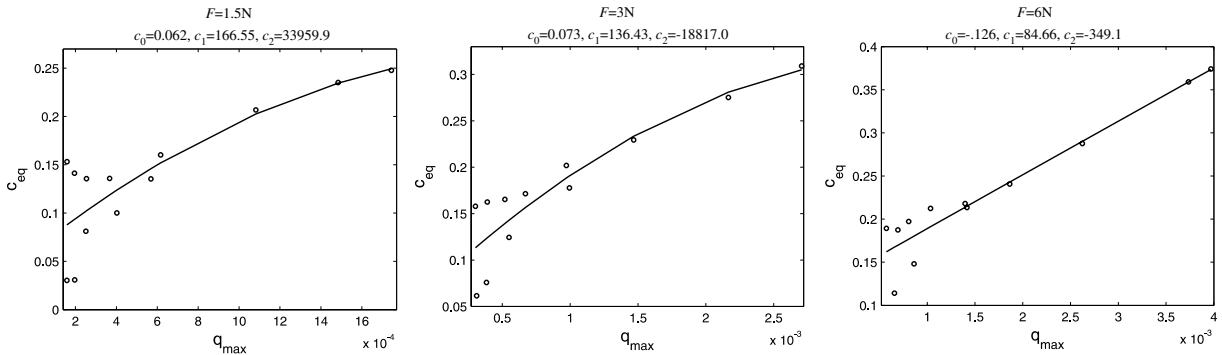

Fig. 13. Identified damping coefficients for preload 120 N: experimental (points) and fitted (full line).
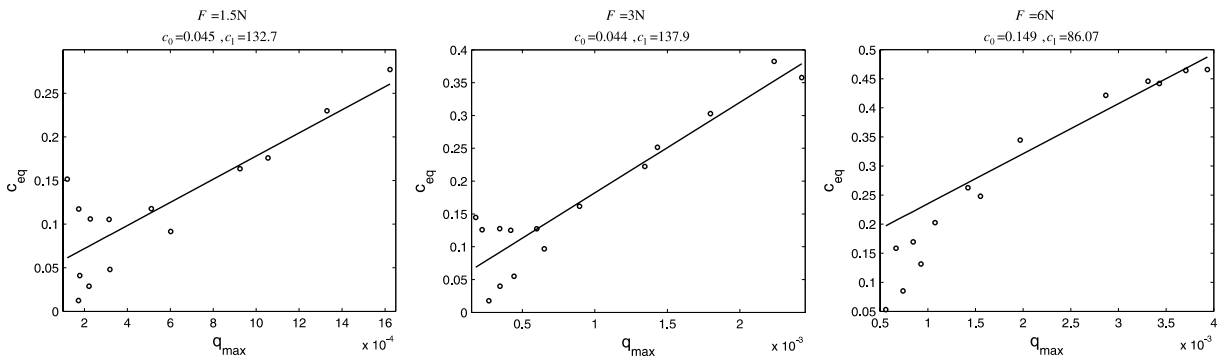

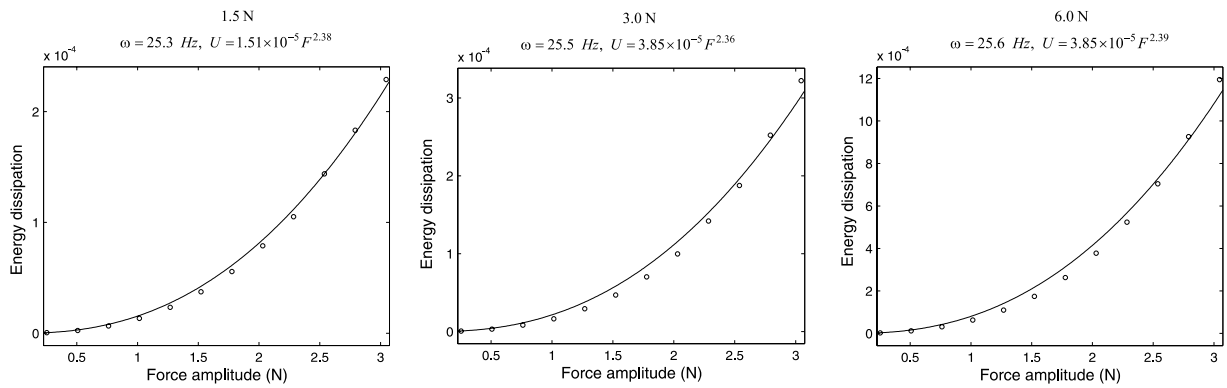Fig. 14. Identified damping coefficients for preload 540 N: experimental (points) and fitted (full line).

Fig. 15. Energy dissipation vs. force amplitude for preload 120 N: calculated (points) and fitted (full line).
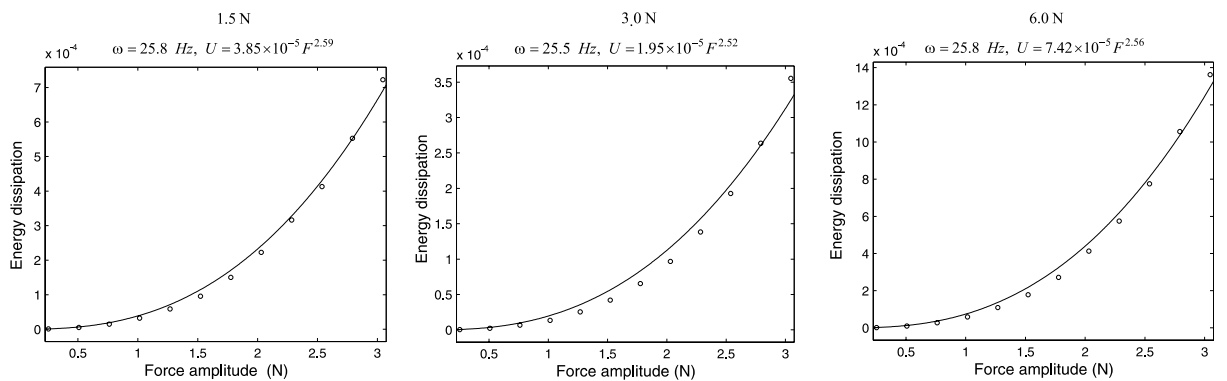

Fig. 16. Energy dissipation vs. force amplitude for preload 540 N: calculated (points) and fitted (full line).

shown with a full line, are produced from the filtered time signals and the analytical loops, in the dashed line, are obtained from the identified parameters – also based on the filtered time-series data. In both figures the two sets of loops, experimental and analytical, show the same basic shape, have the same orientation and the area enclosed appears to be similar. The experimental loops do however appear to contain more exaggerated shapes than the analytical curves, which seems to indicate an underestimation of the cubic stiffness coefficient, k_3. Presumably a better estimate would be determined if the fifth and higher harmonics had not been removed by the filter. Nevertheless the hysteresis curves from both preload conditions provide very good confirmation of the identified cubic stiffness and viscous damping terms dependent upon displacement amplitude. It is of interest to see a hysteresis loop produced from an unfiltered signal. Such a loop is shown in Fig. 19 together with the corresponding filtered version of the same loop. It can be observed that the higher harmonics do indeed have a significant effect.

It should be noted that the identified parameters are meaningful only for motion in the first mode. Different modal parameters would be obtained for the second and higher modes. Physical-coordinate nonlinear parameters could be approximated after obtaining the modal-coordinate nonlinear parameters for several modes and using $\mathbf{d} = \Phi\mathbf{p}$. However, when the excitation frequency is close to a single natural frequency, or in the range of just a few natural frequencies, then the identified modal nonlinear parameters, as described in this paper, will be sufficient to describe the dynamic behaviour of the system.

7. Conclusion

A nonlinear single degree of freedom model in the first modal coordinate was used as the governing equation of a bolted-joint interface between two beams. Filtered steady-state vibration responses to single-
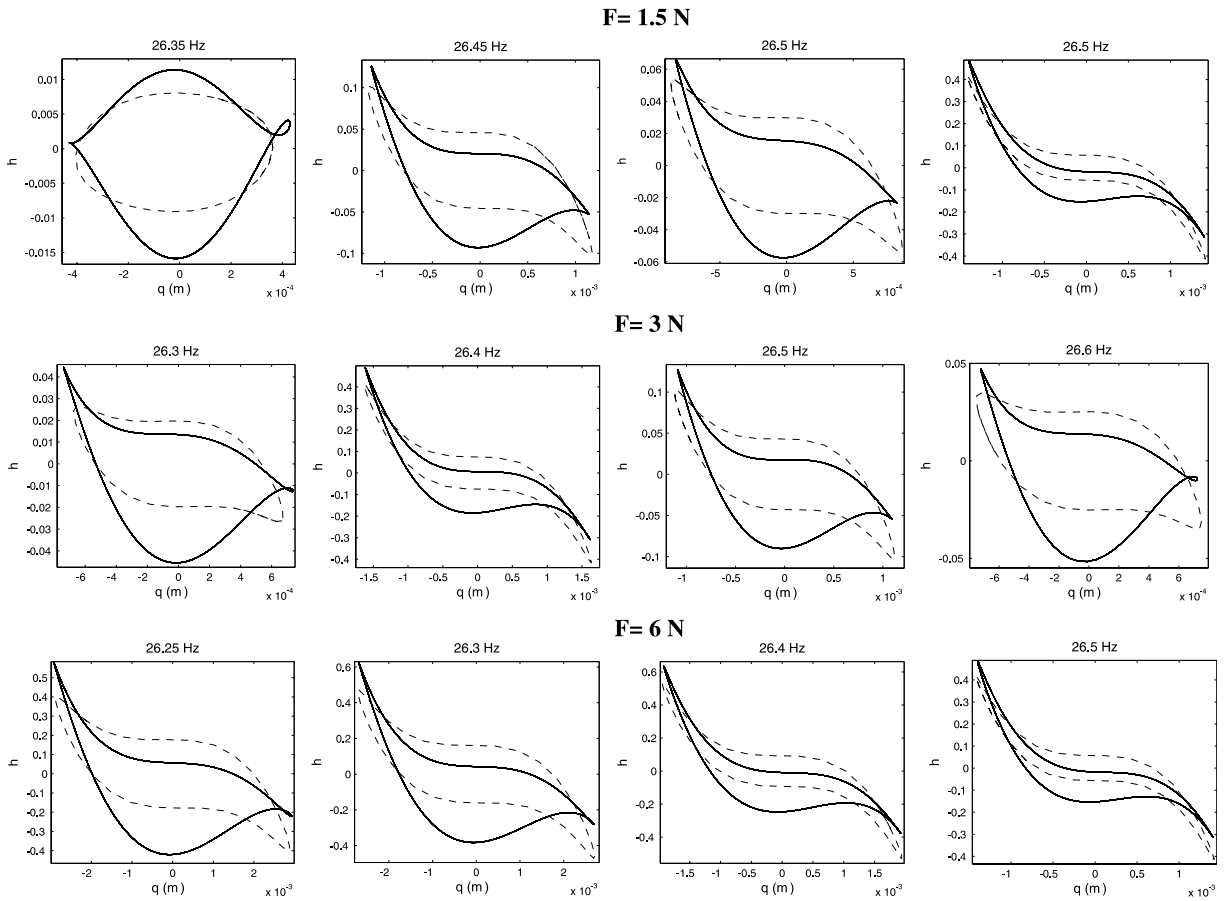
Fig. 17. Hysteresis loops: preload = 120 N.

frequency excitation close to the first natural frequency were used to determine the parameters of the nonlinear model. The identified parameters of the joint model confirmed the presence of both a cubic softening spring and a damping coefficient dependent upon vibration amplitude. Coefficients up to the quadratic in the displacement amplitude were determined. Hysteresis plots reconstructed from the identified parameters were found to show good agreement with measured hysteresis curves. The higher harmonics that had been removed by the filter were shown to add further complexity (curviness) to the hysteresis loops. Never-the-less the hysteresis loops provided considerable validation of the identified cubic stiffness and viscous damping terms dependent upon displacement amplitude.

Appendix A

This section derives the model given in Eq. (12) for primary resonant motion of the jointed structure.

The model shown in Fig. 2 is excited near the first natural frequency. The deformation of the structure when it behaves linearly is expressed using its first mode shape defined as,

$$\varphi_1(x) = \begin{cases} \varphi_{1l}(x), & 0 \leqslant x \leqslant \frac{L}{2} \\ \varphi_{1r}(x), & \frac{L}{2} \leqslant x \leqslant L \end{cases}, \tag{A1}$$

where φ_{1l} and φ_{1r} correspond, respectively, to the left and right hand side substructure deformations of the jointed model. The governing Eq. (1) can be rewritten in the following form:

$$\boldsymbol{\Gamma}_D \mathbf{d} = \bar{\mathbf{f}}, \quad \boldsymbol{\Gamma}_J \mathbf{d} = 0, \quad \boldsymbol{\Gamma}_B \mathbf{d} = 0. \tag{A3–A5}$$

F= 1.5 N
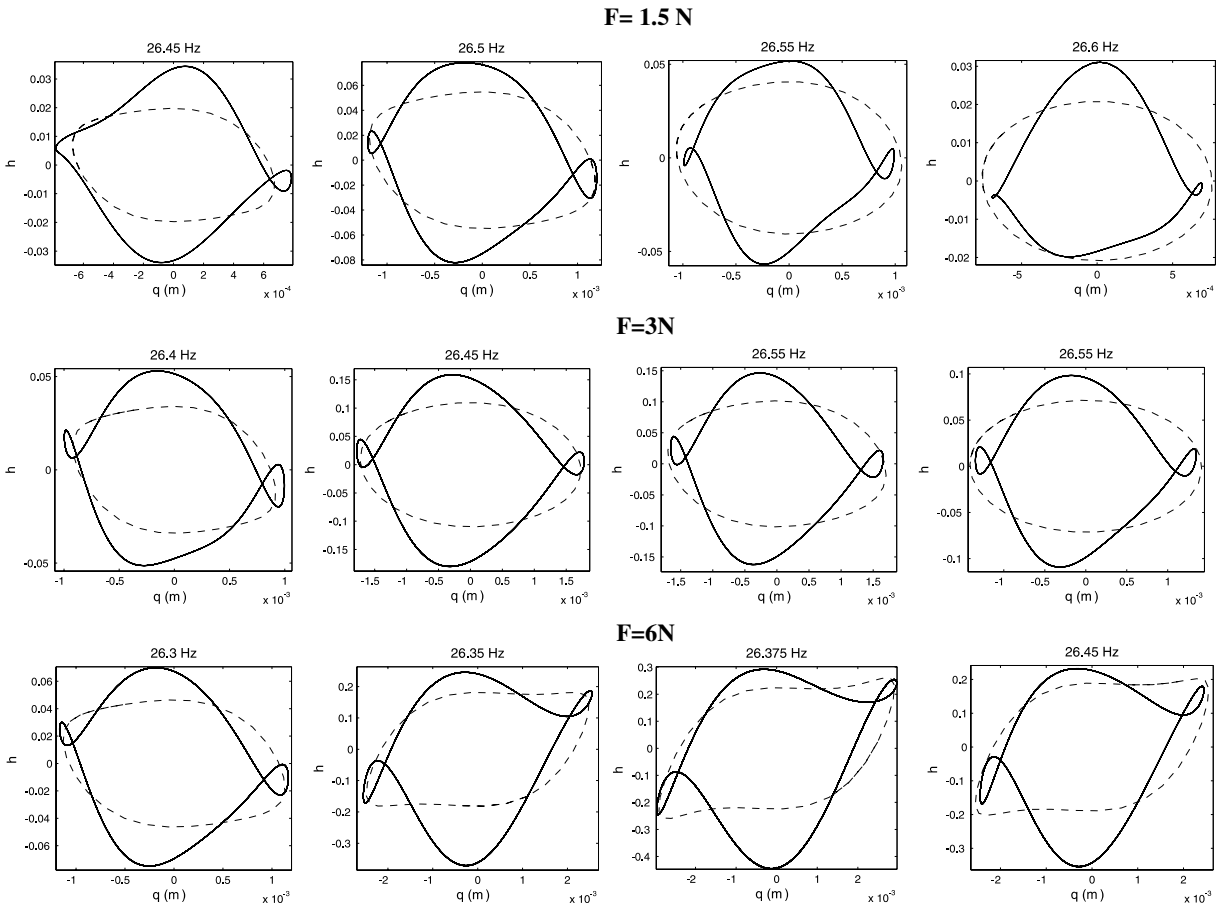

F=3N

F=6N

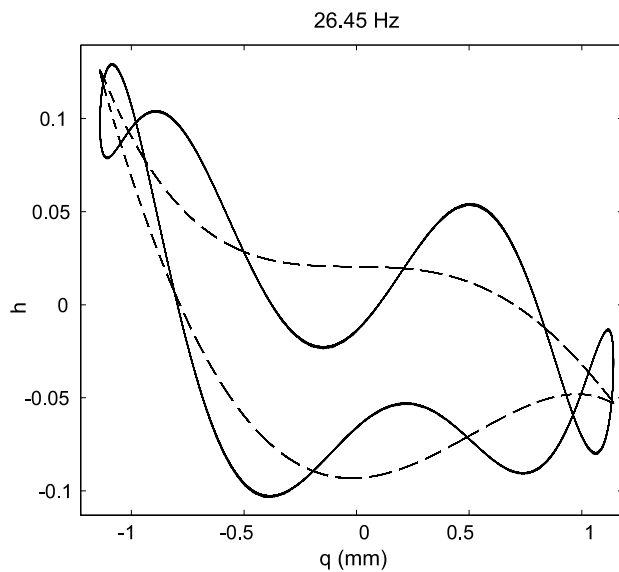

Fig. 18. Hysteresis loops: preload = 540 N.

Fig. 19. Experimental hysteresis loops, filtered (dashed line) and unfiltered (solid line): preload = 120 N.

These equations represent the equation of motion, the joint compatibility requirements and the boundary conditions separately. Transforming (A3) to the modal domain using the transformation given in Eq. (11) results,

$$EI\left(\int_0^{\frac{L}{2}} \varphi_{1l}(x)\frac{\mathrm{d}^4\varphi_{1l}(x)}{\mathrm{d}x^4}\mathrm{d}x + \int_{\frac{L}{2}}^L \varphi_{1r}(x)\frac{\mathrm{d}^4\varphi_{1r}(x)}{\mathrm{d}x^4}\mathrm{d}x\right)q(t) + \rho A\left(\int_0^{\frac{L}{2}} \varphi_{1l}^2(x)\mathrm{d}x + \int_{\frac{L}{2}}^L \varphi_{1r}^2(x)\mathrm{d}x\right)\ddot{q}(t)$$
$$= \left(\int_0^{\frac{L}{2}} \varphi_{1l}(x)f_1(x,t)\mathrm{d}x + \int_{\frac{L}{2}}^L \varphi_{1r}(x)f_2(x,t)\mathrm{d}x\right). \tag{A6}$$

It is assumed the first mode shape is normalized such that the modal mass in Eq. (A6) is unity and the modal force is represented by $Q(t)$. The modal stiffness term in Eq. (A6) is integrated by parts twice, to obtain,

$$EI\left(\int_0^{\frac{L}{2}} \varphi_{1l}(x)\frac{\mathrm{d}^4\varphi_{1l}(x)}{\mathrm{d}x^4}\mathrm{d}x + \int_{\frac{L}{2}}^L \varphi_{1r}(x)\frac{\mathrm{d}^4\varphi_{1r}(x)}{\mathrm{d}x^4}\mathrm{d}x\right)$$
$$= EI\int_0^{\frac{L}{2}}\left(\frac{\mathrm{d}^2\varphi_{1l}(x)}{\mathrm{d}x^2}\right)^2\mathrm{d}x - \left\{\begin{array}{c}\varphi_{1l}(x)\\ \frac{\mathrm{d}\varphi_{1l}(x)}{\mathrm{d}x}\end{array}\right\}^{\mathrm{T}} EI\left\{\begin{array}{c}-\frac{\mathrm{d}^3\varphi_{1l}(x)}{\mathrm{d}x^3}\\ \frac{\mathrm{d}^2\varphi_{1l}(x)}{\mathrm{d}x^2}\end{array}\right\}\Bigg|_0^{\frac{L}{2}} \tag{A7}$$
$$+ EI\int_{\frac{L}{2}}^L\left(\frac{\mathrm{d}^2\varphi_{1r}(x)}{\mathrm{d}x^2}\right)^2\mathrm{d}x - \left\{\begin{array}{c}\varphi_{1r}(x)\\ \frac{\mathrm{d}\varphi_{1r}(x)}{\mathrm{d}x}\end{array}\right\}^{\mathrm{T}} EI\left\{\begin{array}{c}-\frac{\mathrm{d}^3\varphi_{1r}(x)}{\mathrm{d}x^3}\\ \frac{\mathrm{d}^2\varphi_{1r}(x)}{\mathrm{d}x^2}\end{array}\right\}\Bigg|_{\frac{L}{2}}^L.$$

Considering boundary conditions defined in Eq. (A4) the modal stiffness term given in Eq. (A7) can be simplified to,

$$EI\int_0^{\frac{L}{2}}\left(\frac{\mathrm{d}^2\varphi_{1l}(x)}{\mathrm{d}x^2}\right)^2\mathrm{d}x + EI\int_{\frac{L}{2}}^L\left(\frac{\mathrm{d}^2\varphi_{1r}(x)}{\mathrm{d}x^2}\right)^2\mathrm{d}x - \left\{\begin{array}{c}\varphi_{1l}(L/2)\\ \varphi'_{1l}(L/2)\\ \varphi_{1r}(L/2)\\ \varphi'_{1r}(L/2)\end{array}\right\}^{\mathrm{T}}\left\{\begin{array}{c}V_l\\ M_l\\ V_r\\ M_r\end{array}\right\}, \tag{A8}$$

where $V_i, M_i, i = l, r$ correspond to the shear forces and bending moments at the left and the right side of the joint interface. As expected Eq. (A8) shows that the modal stiffness term is equivalent to the strain energy stored in the joint interface and the beam substructures. When the joint interface behaves linearly the modal stiffness is equal to the natural frequency squared, ω_1^2, and Eq. (A1) is represented by a single degree of freedom linear model in modal domain. In the presence of nonlinear joint mechanisms, the equation of motion is changed to,

$$\ddot{q}(t) + \omega_1^2 q(t) + [\varphi_J]\mathbf{f}_J = Q(t), \tag{A9}$$

where $[\varphi_J] = [\varphi_{1l}(L/2) \quad \varphi'_{1l}(L/2) \quad \varphi_{1r}(L/2) \quad \varphi'_{1r}(L/2)]$, and $\mathbf{f}_J$ is the shear force and bending moment produced due to nonlinearity in the joint interface,

$$\mathbf{f}_J = \left\{\begin{array}{c}V_l\\ M_l\\ V_r\\ M_r\end{array}\right\}_{\mathrm{nonlinear}} = \left\{\begin{array}{c}f_1(d_J,\dot{d}_J)\\ g_1(d_J,\dot{d}_J)\\ f_2(d_J,\dot{d}_J)\\ g_2(d_J,\dot{d}_J)\end{array}\right\}. \tag{A10}$$

A similar procedure can be followed to obtain the single mode behavior of the jointed structure when the joint mass and moment of inertia are included in the model as shown in Fig. 3.

References

Ahmadian, H., Jalali, H., 2007a. Identification of bolted lap joints parameters in assembled structures. Mechanical Systems and Signal Processing 21 (2), 1041–1050.

Ahmadian, H., Jalali, H., 2007b. Generic element formulation for modelling bolted lap joints. Mechanical Systems and Signal Processing 21 (5), 2318–2334.

Ahmadian, H., Mottershead, J.E., James, S., Friswell, M.I., Reece, C.A., 2006. Modelling and updating of large surface-to-surface joints in the AWE-MACE structure. Mechanical Systems and Signal Processing 20 (4), 868–880.

Al-Hadid, M.A., Wright, J.R., 1990. Application of the force-state mapping approach to the identification of non-linear systems. Mechanical Systems and Signal Processing 4 (6), 463–482.

Al-Hadid, M.A., Wright, J.A., 1992. Estimation of mass and modal mass in the identification of non-linear single and multi degree of freedom systems using the force-state mapping approach. Mechanical Systems and Signal Processing 6 (4), 383–401.

Berger, E.J., 2002. Friction modeling for dynamic system simulation. Applied Mechanics Reviews 55 (6), 535–577.

Böswald, M., Link, M., 2004. Identification of non-linear joint parameters by using frequency response residuals. In: International Conference on Noise and Vibration Engineering, ISMA, Leuven, Belgium, pp. 3121–3140.

Bucher, I., 1998. Exact adjustment of dynamic forces in presence of non-linear feedback and singularity: theory and algorithm. Journal of Sound and Vibration 218 (1), 1–27.

Dohner, J.L., Gregory, D.L., Segalman, D., Martinez, D.R., 2000. White paper: On the Development of Methodologies for Constructing Predictive Models of Structures with Joints and Interfaces, Structural Dynamics Department, Sandia National Laboratories, Albuquerque, NM.

Ferri, A.A., 1995. Friction damping and isolation systems. Journal of Mechanical Design 117, 196–206.

Ferri, A.A., Bindemann, A.C., 1992. Damping and vibration of beams with various types of frictional support conditions. American Society of Mechanical Engineers. Journal of Vibration and Acoustics 114, 289–296.

Gaul, L., Lenz, J., 1997. Nonlinear dynamics of structures assembled by bolted joints. Acta Mechanica 125 (1–4), 169–181.

Gaul, L., Nitsche, R., 2001. The role of friction in mechanical joints. Applied Mechanics Reviews 52 (2), 93–106.

Goege, D., Fuellekrug, U., Sinapius, M., Link, M., Gaul, L., 2005. Advanced test strategy for identification and characterization of nonlinearities of aerospace structures. AIAA Journal 43 (5), 974–986.

Hartwigsen, C.J., Song, Y., McFarland, D.M., Bergman, L.A., Vakakis, A.F., 2004. Experimental study of non-linear effects in a typical shear lap joint configuration. Journal of Sound and Vibration 277 (1–2), 327–351.

Ibrahim, R.A., Pettit, C.L., 2005. Uncertainties and dynamic problems of bolted joints and other fasteners. Journal of Sound and Vibration 279 (3–5), 857–936.

Ma, X., Bergman, L., Vakakis, A., 2001. Identification of bolted joints through laser vibrometry. Journal of Sound and Vibration 246, 441–460.

Masri, S.F., Caughey, T.K., 1979. A nonparametric identification technique for nonlinear dynamic problems. Journal of Applied Mechanics 46, 433–447.

Masri, S.F., Caffrey, J.P., Caughey, T.K., Smyth, A.W., Chassiakos, A.G., 2004. Identification of the state equation in complex non-linear systems. International Journal of Non-Linear Mechanics 39, 1111–1127.

Mayer, M.A., Gaul, L., 2007. Segment-to-segment contact elements for modelling joint interfaces in finite element analysis. Mechanical Systems and Signal Processing 21, 724–734.

Meskell, C., Fitzpatrick, J.A., 2002. Error in parameter estimates from force state mapping technique for free response due to phase distortion. Journal of Sound and Vibration 252 (5), 967–974.

Meskell, C., Fitzpatrick, J.A., Rice, H.J., 2001. Application of force-state mapping to a non-linear fluid-elastic system. Mechanical Systems and Signal Processing 15 (1), 75–85.

Ouyang, H., Oldfield, M.J., Mottershead, J.E., 2006. Experimental and theoretical studies of a bolted joint excited by a torsional dynamic load. International Journal of Mechanical Sciences 48 (12), 1447–1455.

Segalman, D.J., 2006. Modelling joint friction in structural dynamics. Structural Control Health Monitoring 13, 430–453.

Smallwood, D.O., Gregory, D.L., Coleman, R.G., 2000. Damping Investigations of a Simplified Frictional Shear Joint, Tech. Rep. SAND2000-1929C, Sandia National Laboratories.

Song, Y., Hartwigsen, C.J., McFarland, D.M., Vakakis, A.F., Bergman, A.F., 2004. Simulation of dynamics of beam structures with bolted joints using adjusted Iwan beam elements. Journal of Sound and Vibration 273 (1–2), 249–276.

Ungar, E.E., 1964. Energy dissipation at structural joints: mechanisms and magnitudes, Technical Report FDL-TDR-64-98, U.S. Air Force Flight Dynamics Laboratory.

Ungar, E.E., 1973. The status of engineering knowledge concerning the damping of built-up structures. Journal of Sound and Vibration 26 (1), 141–154.

Worden, K., 1990a. Data processing and experiment design for the restoring force surface method, part I: integration and differentiation of measured time data. Mechanical Systems and Signal Processing 4 (4), 295–319.

Worden, K., 1990b. Data processing and experiment design for the restoring force surface method, part II: choice of excitation signal. Mechanical Systems and Signal Processing 4 (4), 321–344.

Worden, K., Tomlinson, G.R., 2001. Nonlinearity in Structural Dynamics-detection, Identification and Modeling. Institute of Physics Publishing, Bristol, Philadelphia.